ACS APPLIED MATERIALS & INTERFACES

Research Article

www.acsami.org

# $TiO_2$-Assisted Photoisomerization of Azo Dyes Using Self-Assembled Monolayers: Case Study on *para*-Methyl Red Towards Solar-Cell Applications

Lei Zhang[†] and Jacqueline M. Cole*[,†,‡]

[†]Cavendish Laboratory, University of Cambridge, J. J. Thomson Avenue, Cambridge, CB3 0HE, United Kingdom

[‡]Argonne National Laboratory, 9700 S Cass Avenue, Argonne, Illinois 60439, United States

Supporting Information

**ABSTRACT:** The optical and electronic properties of a $TiO_2$ nanoparticle-assisted photo-isomerizable surface, prepared by an azo dye/$TiO_2$ nanocomposite film, are examined experimentally and computationally. The azo dye, *para*-methyl red, undergoes photoisomerization at room temperature, catalyzed by the $TiO_2$ nanoparticle supports, while it exhibits negligible photoisomerization in solvents under otherwise identical conditions. Density functional theory and time-dependent density functional theory are employed to explain the origin of this photoisomerization in these dye···$TiO_2$ nanoparticle self-assembled monolayers (SAMs). The device performance of these SAMs when embedded into dye-sensitized solar cells is used to further elucidate the nature of this azo dye photoisomerization and relate it to the ensuing optoelectronic properties.

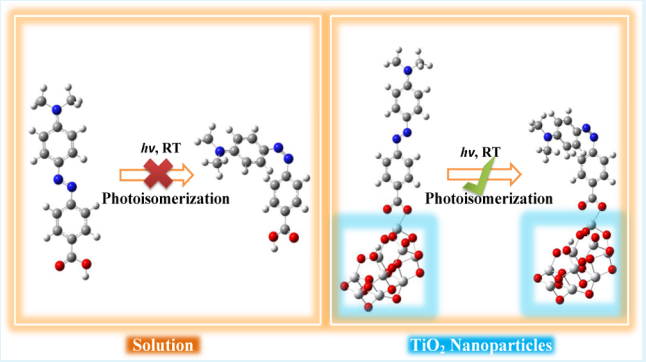


**KEYWORDS:** *photoisomerization, smart surface design, dye-sensitized solar cells, azo dye, optoelectronic materials*

## INTRODUCTION

Smart surface design based on photoisomerizable materials has attracted much attention because of potential applications such as optical data storage, molecular electronics, surface property switching and directed motion on surfaces.[1−3] Azobenzenes, which isomerize between their trans and cis structures (Scheme 1), are probably the most researched compounds in this field, with studies reporting photoisomerization-modulated properties in various states such as in solution, Langmuir−Blodgett film and polymers.[4] Photoisomerization in solution has been studied extensively, but solution-based applications are limited by intrinsic problems of this phase;[5] in addition, many dyes with suitable molecular structures exhibit no photochromism at room temperature in solution, judging from UV/vis absorption spectra, for reasons such as dominant thermal isomerization in such a state.[6]

**Scheme 1. Photoisomerization of *para*-Methyl Red Triggered by UV/Vis Light**

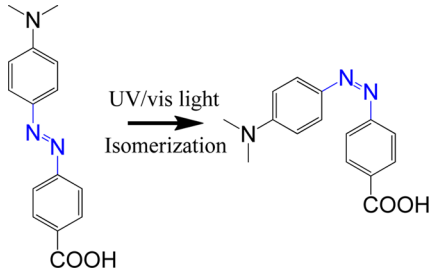


Self-assembled monolayers (SAMs) of azobenzene compounds, on the other hand, exhibit various advantages for room-temperature applications because of their unique properties.[7] Most research in this field use silica or gold nanoparticles as a substrate to which azo dyes self-assemble.[8−10] A terminal thiol group is usually incorporated onto the dye structure so the dye will anchor to the substrate.[11] In contrast, the photoisomerization of azo dyes on $TiO_2$ nanoparticles has been much less explored compared with those on gold particles and in solution.[12]

Recently there has been a renaissance of research on $TiO_2$ nanoparticles due to emerging fields such as dye-sensitized solar cells (DSSCs), which employ a photosensitizer to absorb sunlight and transfer electrons to a $TiO_2$ semiconductor to which the dye is adsorbed.[13−19] Thanks to the development of DSSCs, many anchoring groups are available when the gold nanoparticles are replaced by $TiO_2$ nanoparticles, such as carboxylate, phosphonate, salicylate, sulfonate, acetylacetonate, perylene, nitro, phosphonate, pyridine, siloxane, and hydroxamate groups.[20−24] This provides far greater freedom in

Received: January 18, 2014
Accepted: February 13, 2014
Published: February 13, 2014

  

material selection to design future molecular switches compared with the singular choice of a thiol group as an anchor to the gold. As a result, it would be interesting to explore such azo/$TiO_2$ nanosystems from both a smart surface design (photoisomerization) and optoelectronic (DSSC) point of view.

In this paper, we explore a dye from the pseudostilbene family of azo compounds: 4-[2-[4- (dimethylamino)phenyl]-diazenyl]-benzoic acid (hereafter *para*-methyl red, Scheme 1). This dye possesses a −COOH anchoring group by which it can immobilize the dye on $TiO_2$ nanoparticles as a self-assembled monolayer (SAM). We first demonstrate that this dye undergoes light-stimulated trans → cis photoisomerization when adsorbed onto $TiO_2$ nanoparticles; yet, the dye exhibits negligible photoisomerization in solution at room temperature, evidenced by previous research[25,26] and an in-house UV/vis absorption spectrum obtained in DMSO solvent at room temperature. Complementary density functional theory (DFT) and time-dependent density functional theory (TDDFT) are then used to elucidate the mechanistic origins of the $TiO_2$-assisted photoisomerization in this film. Because of the structural similarity of these SAMs to dye-sensitized $TiO_2$ working electrodes in DSSCs, the azo/$TiO_2$ system was directly incorporated into a DSSC to analyze its optoelectronic properties.

## EXPERIMENTAL AND COMPUTATIONAL METHODS

**Fabrication and Optical Characterization of Photoresponsive Azo Dye/$TiO_2$ Nanocomposite Films.** $TiO_2$ paste (DSL 18NR-T) consisting of 20 nm diameter nanoparticles was purchased from Dyesol. A $TiO_2$ film was deposited onto a glass slide via the doctor-blade method and sintered at 500 °C for 30 min. Sensitization was achieved by dipping the film in a 0.05 mM solution of *para*-methyl red in acetone for five seconds. The resulting nanocomposites on glass were rinsed in ethanol to ensure a monolayer.

UV/vis absorption spectra of the nanocomposite film were obtained using an Agilent8453 Diode Array Spectrophotometer, under both 450 nm peak irradiation (Thorlab, ca. 7 mW $cm^{-2}$) and solar irradiation (ABET Sun 2000 solar simulator, 100 mW $cm^{-2}$).

**DSSC Fabrication and Photovoltaic Characterization.** The preparation of the working electrodes for DSSCs was similar to that of the nanocomposites described above, except the sensitization time was 1 day, the dye concentration was 0.5 mM and the substrate was FTO coated glass (TEC15, Dyesol). The counter-electrodes were prepared via the same doctor-blade method, using chloroplatinic acid hexahydrate ($H_2PtCl_6{\cdot}6H_2O$) from Sigma Aldrich. Each cell was sealed with a 25 $\mu$m thick film of Surlyn, with an electrolyte consisting of a 50 mM iodide/tri-iodide redox couple in acetonitrile solution.

*J*−*V* characteristic responses of the cell incorporating the azo dye/$TiO_2$ nanocomposites were determined using the aforementioned ABET Sun 2000 solar simulator under AM 1.5 illumination at 100 mW $cm^{-2}$.

**Computational Studies.** In order to understand the $TiO_2$-assisted photoisomerization and optoelectronic properties of the azo dye, four input structures (trans, cis, transTiO$_2$ and cisTiO$_2$; see Figure 1), were optimized in Gaussian 09[27] using a B3LYP functional[28] and 3-21g*[29]/6-31g(d,p)[30] basis sets in vacuo. The former two structures are free azo dye isomers while the latter two are the nanocomposites consisting of the free isomer adsorbed onto a $(TiO_2)_9$ nanocluster. The azo dyes adsorb onto the $TiO_2$ surface through the carboxylic group. A diffusing 6-31+g(d,p) basis set was also employed on trans and cis organic molecules. The coordinates of the $(TiO_2)_9$ cluster used in this study are taken from the literature.[31] It has been demonstrated that this size of $TiO_2$ nanocluster is large enough to reproduce the electronic and optical properties of the nanocomposites.[32]

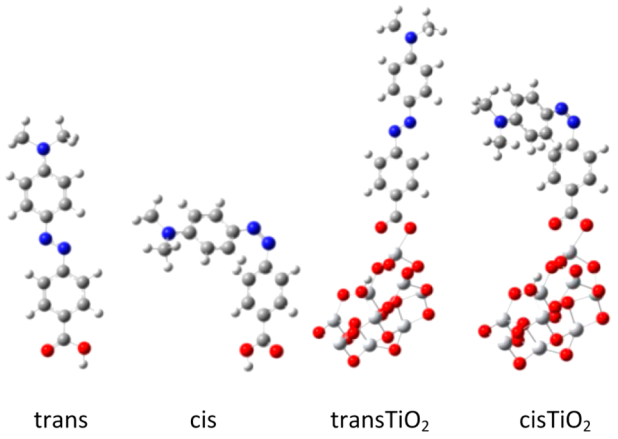


**Figure 1.** DFT-optimized structures for trans, cis, transTiO$_2$ and cis TiO$_2$. Red, oxygen; blue, nitrogen; grey, carbon; small white, hydrogen; large white, titanium.

There are controversies surrounding the exact anchoring modes for dyes on $TiO_2$ nanoparticles; generally, bidentate anchoring modes are considered more stable than other anchoring modes such as monodentate;[33] here we assume a bidentate chelating anchoring mode in accordance with similar organic dyes on the same cluster.[31] Energy levels and distributions of frontier orbitals were plotted and visualized in GaussView.[34] Theoretical UV/vis absorption spectra were computed via TDDFT using the B3LYP/6-31g(d,p) functional and basis set, based on the optimized ground state structures at the same level of theory.

To determine the origin of the $TiO_2$-assisted photoisomerization, the potential energy of the associated C−N=N−C dihedral angle was scanned,[35−37] for both the free dye in DMSO and the dye/$TiO_2$ system, using a B3LYP functional and 6-31g* basis set. Solvent effects were evaluated using the Polarizable Continuum Model.[38] Ground-state (S0) energy was determined by constraining the C−N=N−C dihedral angle while allowing the rest of the molecule to relax. The first (S1), second (S2), and third (S3) excited states were obtained via TDDFT calculations.

## RESULTS AND DISCUSSION

**Trans−Cis Photoisomerism of Azo Dye/$TiO_2$ Nanocomposites.** *para*-Methyl red adsorbed onto $TiO_2$ nanoparticles clearly exhibits photoisomerization (Figures 2 and 3)

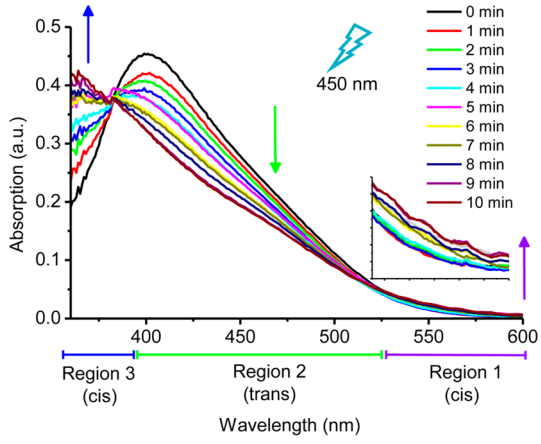


**Figure 2.** UV/vis absorption spectra under 450 nm stimulated optical irradiation at different times. The changes of intensity are indicated by arrows: the intensity increases in region 1 and 3, and decreases in region 2. Inset: magnified view of the absorption spectra in region 1.


dx.doi.org/10.1021/am500308d | ACS Appl. Mater. Interfaces 2014, 6, 3742−3749

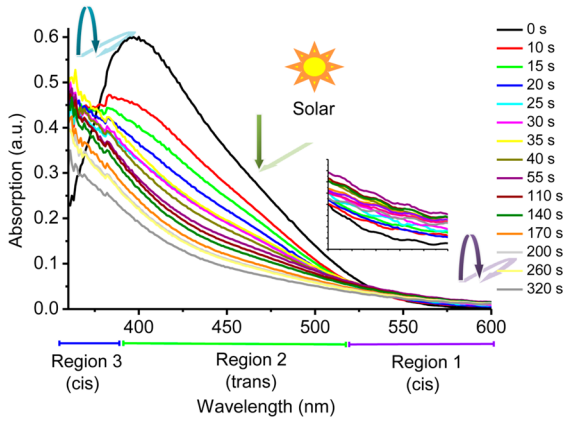


**Figure 3.** UV/vis absorption spectra under solar (100 mW/cm$^2$) stimulation versus irradiation time. The intensities in regions 1 and 3 increase and those in region 2 decrease, indicating trans → cis photoisomerization; after ca. 1 min, all regions exhibit intensity decrease. Inset: magnified view of the absorption spectra in region 1.

under both single wavelength and broad solar irradiation conditions, compared with its negligible photoisomerization/photochromism observed in solution under otherwise identical experimental conditions. The isomerization in this simple nanocomposite system produces similar spectra to those of host-guest structures with an amphiphilic cyclodextrin derivative host by Yabe et al.,[25,26] who acquired low temperature UV/vis absorption of the guest, *para*-methyl red, in solution; the resulting peak at 448 nm was assigned to the trans isomer, whereas peaks at 500 nm and 378 nm were attributed to the cis isomer. We follow this assignment for the nanocomposite film, where region 2 corresponds to changes to the trans isomer whereas region 1 & 3 is characteristic of the cis isomer. In fact, TDDFT calculations will herein confirm the transferability of this spectral assignment from solution to film (vide infra).

Three regions in the visible regime associated with photoisomerization can be identified under light irradiation in Figures 2 & 3, as located by the arrows: region 1 (> ca. 530 nm; cis), region 2 (from ca. 360 nm to ca. 530 nm; trans) and region 3 (< 360 nm; cis). As the incident light with peak at 450 nm shines onto the nanocomposites, the absorption intensity decreases in region 2 and increases in region 1 and 3 (Figure 2), indicating trans → cis photoisomerization catalyzed by $TiO_2$ nanoparticles.

The nanosystem under investigation in this study exhibits irreversible trans → cis photoisomerization, as no cis → trans photoisomerization was evident after solvent, light, and heat have been applied, compared with reversible organics.[19] Pending further examination of other stimuli such as pressure, magnetic or electric fields, pH, or mechanical forces, the irreversible photoswitching of surfaces could be useful in photolithography, in which the patterned modification of a surface can be achieved using masks.[5]

Under solar stimulation (AM 1.5, with photon flux peak ca. 400−800 nm), the UV/vis absorption pattern of the dye/$TiO_2$ system (Figure 3) is similar to that under single wavelength light (Figure 2), although the process of the former is slightly complicated due to much stronger incident flux. The light absorption in region 1 and 3 increases whereas that in region 2 decreases; the process is much faster, compared to the case of 450 nm light stimulation, because of the greater intensity and a broader energy distribution of photons here. In addition, the intensity in regions 1 and 3 decreases again after ca. 1 min, possibly because of $TiO_2$-assisted photocatalytic degradation.[12]

**Comparison of DFT-Optimized Structures.** The DFT-optimized structures, shown in Figure 1, were used to compare bond lengths and angles of the two pairs of cis and trans structures. Both trans and trans$TiO_2$ are extremely planar compared with the twisted cis and cis$TiO_2$ structures: the angle between the two arene rings changes dramatically upon trans-to-cis photoisomerization: from ca. 0° to 68° in the free azo dye (trans to cis) and ca. 0 to 70° when adsorbed on $TiO_2$ (trans$TiO_2$ to cis$TiO_2$) (see Table S1 in the Supporting Information). The bond lengths of the azo group (−N═N−), which are an important indicator of intramolecular charge transfer (ICT) in azo dyes,[39] are comparable between the isomers (1.26−1.27 Å, see Table S1 in the Supporting Information). There are minimal geometrical differences in the conjugated unit between the free molecules and nanocomposites (see Table S1 in the Supporting Information) predicted by DFT calculations, although obvious changes in electronic and optical properties exist (vide infra).

The cation-to-$TiO_2$ surface contact distance (defined and tabulated in Table S1 in the Supporting Information) is 14.15 Å for trans$TiO_2$; this is more than twice that for cis$TiO_2$ (7.04 Å). In a DSSC, the cation-to-semiconductor surface contact distance is closely related to undesirable recombination processes; the open circuit voltage ($V_{oc}$) and short circuit current ($J_{sc}$) decrease with decreasing contact distance, owing to easier electron back transfer to either cation or electro-

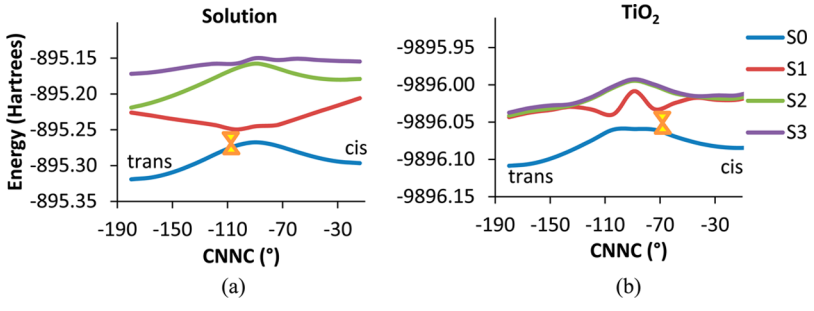


**Figure 4.** Potential energy surface of S0, S1, S2, and S3 for *para*-methyl red (a) in DMSO and (b) on $TiO_2$ in vacuo with respect to CNNC dihedral angles. Trans presents the lowest ground-state energy (the left side of each curve situated at −110°), whereas S0 for cis displays a slightly elevated energy minimum, exclusively in b. An associated pseudo-conical point exists for the dye/$TiO_2$ system near 70°, thereby enabling photoisomerization to the cis$TiO_2$ isomer. The nominal pseudo-conical intersection at −110° in a returns the solution-based system to the trans isomer. Orange double-headed triangles represent the nominal and $TiO_2$-induced pseudo-conical intersections shown in a and b, respectively.

lyte.[33,40] As a result, when adsorbed onto $TiO_2$ nanoparticles, the cis isomer, with its smaller cation-to-$TiO_2$ distance, is expected to exhibit greater recombination and, consequentially, a lower $J_{sc}$ and $V_{oc}$, compared with the trans isomer.

When the free trans dye isomerizes to its cis form, the electrostatic potential (ESP) changes correspondingly, especially in the azo region which becomes more prone to nucleophilic attack (see Figure S1 in the Supporting Information). The change is less obvious when the dye is anchored onto the nanocomposites (see Figure S1 in the Supporting Information), because the interactions between the $TiO_2$ nanoparticles and the organic molecules render the dye molecules more neutral in all regions.

**Potential Energy Surface.** Figure 4 depicts the potential energy of the two isomers (in DMSO and on $TiO_2$ nanoparticles) as a function of C−N═N−C dihedral angle, obtained from DFT/TDDFT. The first- and second-excited states, S1 and S2, are populated via HOMO → LUMO and HOMO-1 → LUMO+1 transitions, respectively, whereas the nature of S3 is representative of transitions from a number of occupied-to-unoccupied molecular orbitals. Three major features in the potential energy scan are noteworthy in Figure 4: firstly, when the dye is adsorbed onto $TiO_2$ nanoparticles, the energy surfaces of these excited states move close to each other, due to extra states introduced by the $TiO_2$ nanoparticles. Secondly, better coupling between different excited states is present for the dye/$TiO_2$ system. This facilitates the decay from higher excited states to the first excited state, at which the de-excitation to S0 occurs; while the nominal S1 → S0 decay pathway (lowest energy) lies at approximately −110°. Third, and most importantly, the S1 state of the azo dye/$TiO_2$ system has an additional energy minimum at a C−N═N−C angle of around −70°, which corresponds closely to that of the characteristic cis isomer; this point acts as a pseudo-conical intersection to enable a new decay pathway from the S1 to S0 potential energy surface; given the dihedral angle associated with this decay, the system relaxes into the cis structure. This explains how the $TiO_2$ nanoparticles assist the photoisomerization from the trans to cis isomer. The absence of this energy minimum when the dye exists in solution (DMSO) leaves the nominal pseudo-conical intersection at ∼110° as the favored decay pathway, rendering a return to the trans state (i.e., no photoisomerization occurs in solution).

The fact that this additional pseudo-conical intersection point serves as an energy trap such that relaxation goes to the cis structure might also be partly responsible for the irreversible photoisomerization of the azo dye/$TiO_2$ system. Even though the trans form has a lower overall energy than the cis isomer, the energy barrier of S0 for the azo dye/$TiO_2$ system has a large thermal barrier (ca. 0.7 eV); this prevents thermal isomerization from cis$TiO_2$ to trans$TiO_2$. Another possible hindrance to the cis → trans isomerization is the compact nature of the cis structure,[10] which might be overcome by further molecular engineering such as tripodal and alkane introduction to achieve a free volume increase.[24]

**Frontier Molecular Orbitals.** The nature of frontier molecular orbitals is a crucial indicator of optical and optoelectronic properties.[41] Selected orbital distributions for trans$TiO_2$ and cis$TiO_2$ are plotted in Figure 5. The virtual orbital distributions of LUMO and LUMO+1 demonstrate that photo-absorbed charge localization will predominantly reside in the $TiO_2$ cluster, rather than in the organic molecules. This indicates efficient electron injection into the bulk semiconductor. In contrast, electronic charge in the HOMO (the dialkyl nitrogen and the ring attached to it) is mainly located in the region furthest from the $TiO_2$ surface, while charge in the HOMO-1 is mainly located in the azo group. These HOMO and HOMO-1 distributions exhibit relatively few changes compared to the free molecule, unlike their LUMO counterparts (see the Supporting Information, Figure S2). The embedding of a $TiO_2$ cluster onto the azo dye therefore induces a significant redistribution of electron density, with the primary changes resting in the LUMOs where the primary orbital populations shift from the dye into the $TiO_2$ cluster.

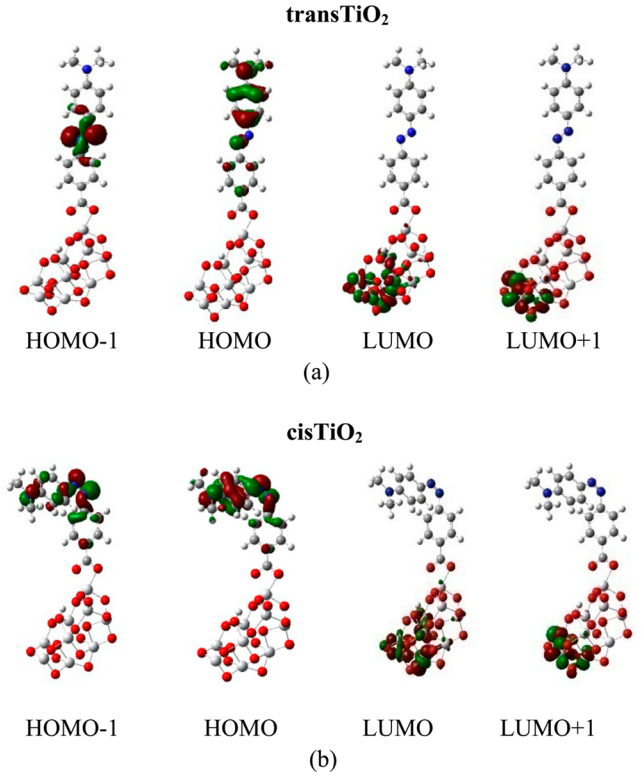


**Figure 5.** Frontier orbital distributions of the HOMO-1, HOMO, LUMO, and LUMO+1 for (a) trans$TiO_2$ and (b) cis$TiO_2$.

The energy levels of molecular orbitals are important for photoelectrochemical device considerations: in a DSSC, the LUMO energy level should be above the bottom of the conduction band (CB) of $TiO_2$ (−-4.04 eV vs. vacuum[42]) for electron injection purposes, and the HOMO level should be lower than the redox level of the electrolyte (−4.94 eV vs. vacuum[42]) for dye regeneration purposes.[43]

Figure 6 indicates that both of the free dye isomers (trans and cis) have LUMO levels (−2.16 eV for trans and −1.91 eV for cis) above the bottom of the CB of $TiO_2$ and HOMO levels (−5.30 eV for trans and −5.28 eV for cis) below the electrolyte redox level; this means that both trans and cis isomers satisfy the energy level criteria for DSSCs. In addition, although cis seems to have a larger driving force for electron injection (a higher LUMO level than that of trans), it exhibits a larger band gap, which is undesirable for optical absorption;[41] indeed, considering the lower optical absorption determined by experiments, with its larger band gap, the cis isomer is inferior to trans in terms of light absorption.

The scenario is similar for the two nanocomposites: the LUMO levels of trans$TiO_2$ and cis$TiO_2$ are higher than the bottom of the $TiO_2$ CB and their HOMO levels are lower than

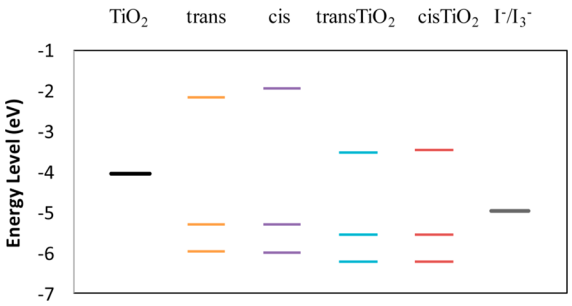


**Figure 6.** Plot of HOMO-1 (lowest), HOMO (middle), and LUMO (highest) energy levels of trans, cis, transTiO$_2$ and cisTiO$_2$. Reference values for the bottom of TiO$_2$ conduction band (-4.04 eV) and $I^-/I_3^-$ redox level (−4.94 eV) are taken from the literature[42] and are plotted for comparison.

the electrolyte redox level, indicating a strong driving force for electron injection from nanocomposites to the bulk semiconductor, and favorable regeneration of the neutral dye. There are, however, some differences between the free organic isomers and nanocomposite forms predicted by DFT: the optical band gap is much smaller for the nanocomposites, indicating that dye···TiO$_2$ adsorption has a distinct facilitatory impact on the energy level characteristics required for favorable light absorption; this is also manifest in the UV/vis absorption spectra calculated via TDDFT (Figure 7). Accordingly, the light

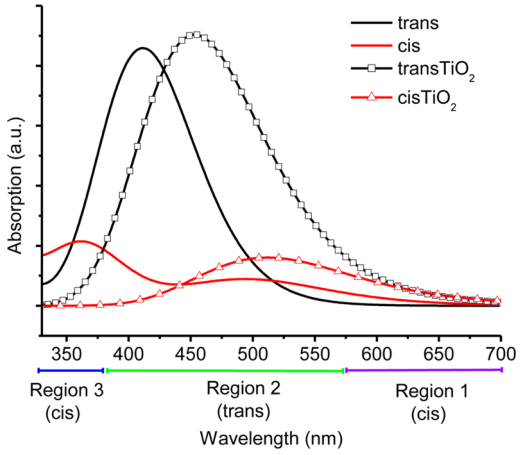


**Figure 7.** Normalized UV/vis absorption spectra calculated by TDDFT at the b3lyp/6-31g(d,p) level. Region 1 essentially comprises cisTiO$_2$ absorption; absorption contributions in region 2 mainly arise from trans and transTiO$_2$; region 3 is dominated by cis absorption (note the subtle larger absorption intensity of cisTiO$_2$ in most of this region).

absorption disadvantages noted for the cis isomer in its free form are essentially negated once they have been incorporated into a dye/TiO$_2$ nanocomposite.

**Simulated UV/Vis Absorption Spectra.** In common with the experimental spectra (Figures 2 and 3), UV/vis absorption spectra of trans, cis, transTiO$_2$, and cisTiO$_2$ predicted by TDDFT (Figure 7) could also be divided into three regions: region 1 (essentially comprising cisTiO$_2$ spectral features), region 2 (dominated by spectral features of trans and transTiO$_2$), and region 3 (dominated by cis), whose wavelengths closely match those of the experimental spectra. These computed trans and cis spectral categorizations confirm the experimental assignments, where region 2 was assigned to trans (more precisely, contributions are from both trans and transTiO$_2$) and region 1 & 3 are assigned to cis (similarly, from both cis and cisTiO$_2$ contributions). As photoirradiation proceeds, trans decreases while cis increases, indicating that intensity in regions 1 and 3 increases while that in region 2 decreases. This was observed experimentally (Figures 2 and 3). In other words, the TDDFT prediction agrees with the experimental photoisomerization data and its corresponding spectral peak assignments.

**Photoisomerization Captured by DSSC Performance.** When the azo dye/TiO$_2$ nanocomposites are deposited onto conducting FTO glass and overlaid with a Pt-coated FTO glass counter electrode, between which is placed a suitable redox electrolyte, a dye-sensitized solar cell is formed (Figure 8). The solar cell provides electrical power and so its photoresponse can give additional diagnostic information about the photoisomerization process of the organic dyes on TiO$_2$ nanoparticles.[19] Usually, longer time evolution (days to months) of cell performance is frequently examined when solar cell stability should be considered,[16,23] but the subtle performance changes at short time span (minutes) are rarely examined. Figure 2 and 3 indicate that the photoisomerization is particularly active within the first few minutes of photoirradiation which might impact on overall cell performance. Figure 9 depicts the $J-V$ curves of the corresponding azo dye/TiO$_2$-incorporated solar cell, measured at different time intervals under solar stimulation. The four critical parameters of cell performance ($J_{sc}$, $V_{oc}$, FF, and $\eta$), plotted as a function of time, are shown in Figure 10. Solar cell performance seems to correlate well with the process of photoisomerization. $J_{sc}$ (electrical short-circuit current density) is largely affected by the light absorption (solar energy). As a result, the time-dependent decrease of absorption in most visible regions, because of a decrease in trans isomer population (Figure 3), leads to a continuous decrease of $J_{sc}$. The decrease of $J_{sc}$ is more obvious in the first minute (Figure 10). $V_{oc}$ is strongly affected by the electron recombination rate to the electrolyte. As was anticipated via the DFT-simulated adsorbed structures, the cis isomer exhibits a larger recombination rate, as the cis isomer adsorbs nearer to the TiO$_2$ surface; correspondingly, the charge density in the HOMO of cisTiO$_2$ lies close to this surface (Figure 5). As a result of the cis formation, $V_{oc}$ decreases over time, especially for the first minute. That said, this observed trend of $V_{oc}$ is similar to that of the protonated form of the celebrated DSSC dye, N719, i.e., N3, under the same short time evolution (see Figure S3 in the Supporting Information). This suggests that purely stabilization effects associated with the different photoelectrochemical processes that govern the cell performance might dominate the nature of $V_{oc}$, rather than photoisomerization. The same holds true for FF and $\eta$ when the azo dye performance is compared with reference N3 dye; nevertheless, the decrease in $J_{sc}$ of the azo dye is dramatically different compared with N3, strongly indicating the impact of photoisomerization on DSSC performance; this agrees with previous findings on other organic dyes.[19,44] It should also be noted that $V_{oc}$ is complicated by a possible effect that the cis structures form a sterically hindered layer on the TiO$_2$ surface (Figure 8a) which stands to block the electron back transfer from the TiO$_2$ region to the electrolyte much more in the cis form than in the trans configuration.

Repetitive device testing in duplicate DSSCs (see Figure S4 in the Supporting Information) indicates that such time revolution trend of $J_{sc}$ is consistent. Although the time

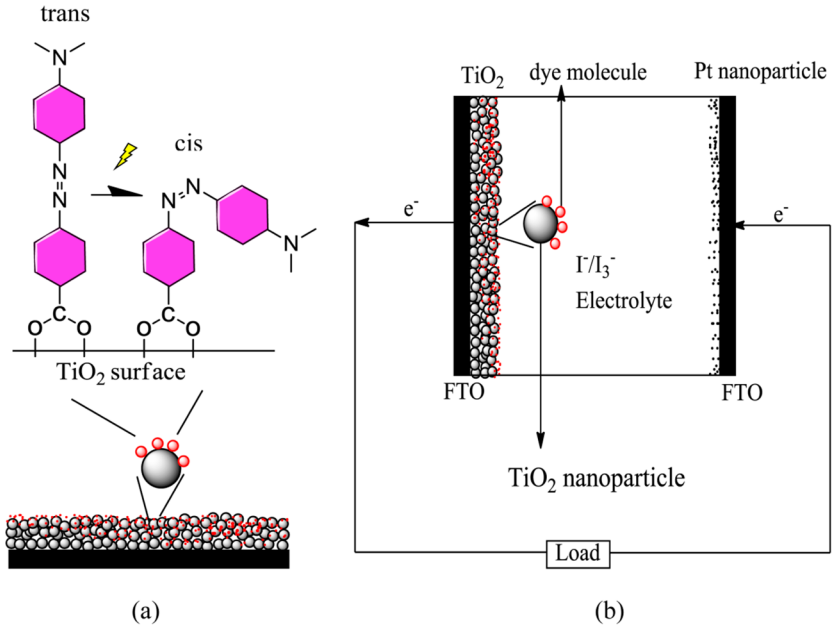


**Figure 8.** Magnified view of (a) trans-to-cis photoisomerization of azo dyes on $TiO_2$ nanoparticles and (b) azo dye/$TiO_2$ nanocomposites embedded in dye-sensitized solar cells. The little red dots represent the azo molecules, whereas the grey colored balls represent $TiO_2$ nanoparticles.

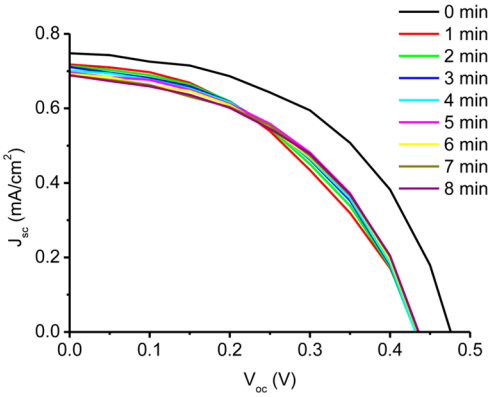


**Figure 9.** $J-V$ curves of the solar cell measured at different times while exposed under a solar simulator. The progressive change in $J-V$ responsive curves is due to photoisomerization of azo dyes.

evolution of DSSC performance could result from a stabilization of other factors, the strong correlation between the UV/vis absorption spectra and $J_{sc}$ time evolution provides a reassuring "diagnosis" of photoisomerization via dye-sensitized solar cell performance.

## CONCLUDING REMARKS

$TiO_2$ nanoparticles have been shown to assist the trans−cis photoisomerization process of the subject azo dye, evidenced by UV/vis absorption spectra, in stark contrast with the dye in solution where negligible photoisomerization at room temperature exists. DFT/TDDFT calculations provide an explanation for this catalytic action, via the revelation that an additional pseudo-conical intersection point exists near the cis structural configuration when the dye is adsorbed to $TiO_2$ nanoparticles, while in solution the only pseudo-conical intersection point exists near the trans geometry. This additional pseudo-conical intersection offers a de-excitation pathway to a stable cis ground state local minimum.

The photoisomerization of this azobenzene derivative has an evident effect on its photoelectrochemical properties. The photoresponsive changes, unveiled by employing corresponding DSSC photovoltaic characterization as a diagnostic, give further information on the trans-cis photoisomerization of azo dyes. To this end, the step-wise changes in $J-V$ curves shown herein indicate the mechanistic evolution of photoisomerization on the $TiO_2$ surface.

Although the overall DSSC performance suggests that the photoisomerization process impacts detrimentally on the resulting $J_{sc}$, the intricate, more complicated optical and optoelectronic changes of the azo dye should not be neglected. For example, if one can deal with this short timeframe $J_{sc}$ issue,

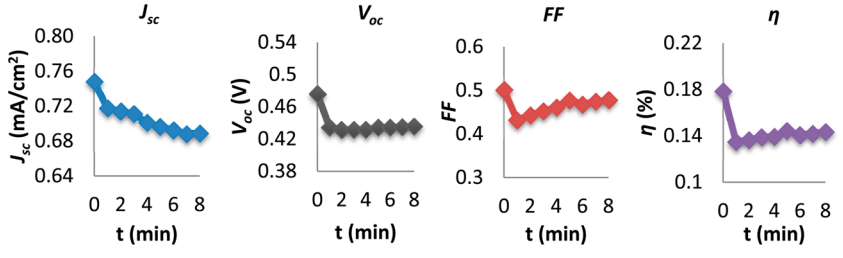


**Figure 10.** $J_{sc}$, $V_{oc}$, FF, and $\eta$ as a function of time. $J_{sc}$ continuously decreases especially for the first minute.


dx.doi.org/10.1021/am500308d | ACS Appl. Mater. Interfaces 2014, 6, 3742−3749

this $TiO_2$-assisted azo dye photoisomerization could actually realize better panchromatic performance in DSSC technology as the cis and trans isomer mixing would render a form of dye quasi-cosensitization owing to the complementary optical absorption characteristics of each isomer. Moreover, the more optimal geometry of the cis isomer on $TiO_2$ nanoparticles, relative to the trans isomer, suggests a compact layer formation that sterically inhibits losses owing to dark current.

In more general terms, this subject dye serves as an exemplar in the sense that $TiO_2$ nanoparticles could activate many photoisomerizable azo-dye compounds as long as anchoring groups such as carboxylate, phosphonate, sulfonate, pyridine, perylene and hydroxamate are employed; this prospects the greater freedom in material selection for the design of future azo-dye based molecular switches. Pending the trans−cis irreversibility shown in this subject case can be circumvented by judicious tuning of the pseudo-conical intersection via chemical substitution, such molecular switching could be tailored to be reversible, or irreversible, to suit a given device application. Combining this with the fact that a large pool of anchors could be used to immobilize organics onto the $TiO_2$ surface, in contrast to the gold nanoparticle thiol anchoring restrictions, the future molecular design of photoisomerizable smart surfaces could be facilitated.

## ■ ASSOCIATED CONTENT

### Supporting Information

List of azo bond lengths and angles between two phenyl rings and cation-$TiO_2$ surface distances (Table S1); electrostatic potential for trans, cis, trans$TiO_2$ and cis$TiO_2$ (Figure S1); distributions of HOMO-1, HOMO, LUMO and LUMO+1 orbitals for trans and cis (Figure S2); HOMO-1, HOMO and LUMO energy levels of trans, cis, trans$TiO_2$ and cis$TiO_2$ using different basis sets (Table S2); time evolution of DSSC performance by the reference N3 dye (Figure S3); and multiple testing of a DSSC incorporated with *para*-methyl red (Figure S4). This material is available free of charge via the Internet at http://pubs.acs.org.

## ■ AUTHOR INFORMATION

### Corresponding Author

*E-mail: jmc61@cam.ac.uk. Tel: +44 (0)1223 337470. Fax: +44 (0)1223 337470.

### Author Contributions

The manuscript was written through contributions of all authors. All authors have given approval to the final version of the manuscript.

### Notes

The authors declare no competing financial interest.

## ■ ACKNOWLEDGMENTS

J.M.C. thanks the Fulbright Commission for a UK-US Fulbright Scholar Award hosted by Argonne National Laboratory, where work done was supported by DOE Office of Science, Office of Basic Energy Sciences, under Contract DE-AC02-06CH11357. The authors acknowledge support from the EPSRC UK National Service for Computational Chemistry Software (NSCCS), based at Imperial College London, and contributions from its staff in carrying out this work.

## ■ REFERENCES

(1) Klajn, R.; Stoddart, J. F.; Grzybowski, B. A. Nanoparticles Functionalised with Reversible Molecular and Supramolecular Switches. *Chem. Soc. Rev.* **2010**, *39*, 2203−2237.
(2) Han, M.; Ishikawa, D.; Honda, T.; Ito, E.; Hara, M. Light-Driven Molecular Switches in Azobenzene Self-Assembled Monolayers: Effect of Molecular Structure on Reversible Photoisomerization and Stable Cis State. *Chem. Commun.* **2010**, *46*, 3598−3600.
(3) Kubitschke, J.; Näther, C.; Herges, R. Synthesis of Functionalized Triazatriangulenes for Application in Photo-Switchable Self-Assembled Monolayers. *Eur. J. Org. Chem.* **2010**, *2010*, 5041−5055.
(4) Natansohn, A.; Rochon, P. Photoinduced Motions in Azo-Containing Polymers. *Chem. Rev.* **2002**, *102*, 4139−4176.
(5) Browne, W. R.; Feringa, B. L. Light Switching of Molecules on Surfaces. *Annu. Rev. Phys. Chem.* **2009**, *60*, 407−428.
(6) Bandara, H. M. D.; Burdette, S. C. Photoisomerization in Different Classes of Azobenzene. *Chem. Soc. Rev.* **2012**, *41*, 1809−1825.
(7) Zhang, J.; Whitesell, J. K.; Fox, M. A. Photoreactivity of Self-Assembled Monolayers of Azobenzene or Stilbene Derivatives Capped on Colloidal Gold Clusters. *Chem. Mater.* **2001**, *13*, 2323−2331.
(8) Comstock, M.; Levy, N.; Kirakosian, A.; Cho, J.; Lauterwasser, F.; Harvey, J.; Strubbe, D.; Fréchet, J.; Trauner, D.; Louie, S.; et al. Reversible Photomechanical Switching of Individual Engineered Molecules at a Metallic Surface. *Phys. Rev. Lett.* **2007**, *99*, 038301.
(9) Jung, U.; Kuhn, S.; Cornelissen, U.; Tuczek, F.; Strunskus, T.; Zaporojtchenko, V.; Kubitschke, J.; Herges, R.; Magnussen, O. Azobenzene-Containing Triazatriangulenium Adlayers on Au(111): Structural and Spectroscopic Characterization. *Langmuir* **2011**, *27*, 5899−5908.
(10) Morgenstern, K. Isomerization Reactions on Single Adsorbed Molecules. *Acc. Chem. Res.* **2009**, *42*, 213−223.
(11) Saha, S.; Stoddart, J. F. Photo-Driven Molecular Devices. *Chem. Soc. Rev.* **2007**, *36*, 77−92.
(12) Zhang, H.; Chen, D.; Lv, X.; Wang, Y.; Chang, H.; Li, J. Energy-Efficient Photodegradation of Azo Dyes with $TiO_2$ Nanoparticles Based on Photoisomerization and Alternate UV-Visible Light. *Erviron. Sci. Technol.* **2010**, *44*, 1107−1111.
(13) O'Regan, B.; Grätzel, M. A Low-Cost, High-Efficiency Solar Cell Based on Dye-Sensitized Colloidal $TiO_2$ Films. *Nature* **1991**, *353*, 737−740.
(14) Hardin, B. E.; Snaith, H. J.; McGehee, M. D. The Renaissance of Dye-Sensitized Solar Cells. *Nat. Photonics* **2012**, *6*, 162−169.
(15) Grätzel, M. Photoelectrochemical Cells. *Nature* **2001**, *414*, 338−344.
(16) Kim, S.; Lee, J. K.; Kang, S. O.; Ko, J.; Yum, J.-H.; Fantacci, S.; Angelis, F.; De Censo, D.; Di Nazeeruddin, M. K.; Grätzel, M. Molecular Engineering of Organic Sensitizers for Solar Cell Applications. *J. Am. Chem. Soc.* **2006**, *128*, 16701−16707.
(17) Nazeeruddin, M. K.; Angelis, F.; De Fantacci, S.; Selloni, A.; Viscardi, G.; Liska, P.; Ito, S.; Takeru, B.; Grätzel, M. Combined Experimental and DFT-TDDFT Computational Study of Photoelectrochemical Cell Ruthenium Sensitizers. *J. Am. Chem. Soc.* **2005**, *127*, 16835−16847.
(18) Zhang, L.; Cole, J. M.; Waddell, P. G.; Low, K. S.; Liu, X. Relating Electron Donor and Carboxylic Acid Anchoring Substitution Effects in Azo Dyes to Dye-Sensitized Solar Cell Performance. *ACS Sustain. Chem. Eng.* **2013**, *1*, 1440−1452.
(19) El-Zohry, A.; Orthaber, A.; Zietz, B. Isomerization and Aggregation of the Solar Cell Dye D149. *J. Phys. Chem. C* **2012**, *116*, 26144−26153.
(20) Galoppini, E. Linkers for Anchoring Sensitizers to Semiconductor Nanoparticles. *Coord. Chem. Rev.* **2004**, *248*, 1283−1297.
(21) Brewster, T. P.; Konezny, S. J.; Sheehan, S. W.; Martini, L. A.; Schmuttenmaer, C. A.; Batista, V. S.; Crabtree, R. H. Hydroxamate Anchors for Improved Photoconversion in Dye-Sensitized Solar Cells. *Inorg. Chem.* **2013**, *52*, 6752−6764.
(22) Ooyama, Y.; Inoue, S.; Nagano, T.; Kushimoto, K.; Ohshita, J.; Imae, I.; Komaguchi, K.; Harima, Y. Dye-Sensitized Solar Cells Based

on Donor-Acceptor $\pi$-Conjugated Fluorescent Dyes with a Pyridine Ring as an Electron-Withdrawing Anchoring Group. *Angew. Chem. Int. Ed.* **2011**, *123*, 7567−7571.
(23) Mao, J.; He, N.; Ning, Z.; Zhang, Q.; Guo, F.; Chen, L.; Wu, W.; Hua, J.; Tian, H. Stable Dyes Containing Double Acceptors Without COOH as Anchors for Highly Efficient Dye-Sensitized Solar Cells. *Angew. Chem., Int. Ed.* **2012**, *51*, 9873−9876.
(24) Long, B.; Nikitin, K.; Fitzmaurice, D. Assembly of an Electronically Switchable Rotaxane on the Surface of a Titanium Dioxide Nanoparticle. *J. Am. Chem. Soc.* **2003**, *125*, 15490−15498.
(25) Yabe, A.; Kawabata, Y.; Niino, H.; Matsumoto, M.; Ouchi, A.; Takahashi, H.; Tamura, S.; Tagaki, W.; Nakahara, H.; Fukuda, K. Photoisomerization of the Azobenzenes Included in Langmuir-Blodgett Films of Cyclodextrins. *Thin Solid Films* **1988**, *160*, 33−41.
(26) Niino, H.; Yabe, A.; Ouchi, A.; Tanaka, M.; Kawabata, Y.; Tamura, S.; Miyasaka, T.; Tagaki, W.; Nakahara, H.; Fukuda, K. Stabilization of a Labile Cis-Azobenzene Derivative with Amphiphilic Cyclodextrins. *Chem. Lett.* **1988**, 1227−1230.
(27) Frisch, M. J.; Trucks, G. W.; Schlegel, H. B.; Scuseria, G. E.; Robb, M. A.; Cheeseman, J. R.; Scalmani, G.; Barone, V.; Mennucci, B.; Petersson, G. A.; Nakatsuji, H.; Caricato, M.; Li, X.; Hratchian, H. P.; Izmaylov, A. F.; Bloino, J.; Zheng, G.; Sonnenb, D. J. Gaussian 09, Revision B 01 2009.
(28) Becke, A. D. Density-Functional Thermochemistry. III. The Role of Exact Exchange. *J. Chem. Phys.* **1993**, *7*, 5648−5652.
(29) Gordon, M. S.; Binkley, J. S.; Pople, J. A.; Pietro, W. J.; Hehre, W. J. Self-Consistent Molecular-Orbital Methods. 22. Small Split-Valence Basis Sets for Second-Row Elements. *J. Am. Chem. Soc.* **1982**, *104*, 2797−2803.
(30) Rassolov, V. A.; Ratner, M. A.; Pople, J. A.; Redfern, P. C.; Curtiss, L. A. 6-31G* Basis Set for Third-Row Atoms. *J. Comput. Chem.* **2001**, *22*, 976−984.
(31) Sánchez-de-Armas, R.; San Miguel, M. Á.; Oviedo, J.; Sanz, J. F. Coumarin Derivatives for Dye Sensitized Solar Cells: a TD-DFT Study. *Phys. Chem. Chem. Phys.* **2012**, *14*, 225−233.
(32) Sánchez-de-Armas, R.; Oviedo López, J.; A. San-Miguel, M.; Sanz, J. F.; Ordejón, P.; Pruneda, M. Real-Time TD-DFT Simulations in Dye Sensitized Solar Cells: The Electronic Absorption Spectrum of Alizarin Supported on $TiO_2$ Nanoclusters. *J. Chem. Theory Comput.* **2010**, *6*, 2856−2865.
(33) Hagfeldt, A.; Boschloo, G.; Sun, L.; Kloo, L.; Pettersson, H. Dye-Sensitized Solar Cells. *Chem. Rev.* **2010**, *110*, 6595−6663.
(34) Dennington, R.; Keith, T.; Millam, J.*GaussView*; Gaussian: Wallingford, CT, 2009.
(35) Tiago, M. L.; Ismail-Beigi, S.; Louie, S. G. Photoisomerization of Azobenzene from First-Principles Constrained Density-Functional Calculations. *J. Chem. Phys.* **2005**, *122*, 094311.
(36) Ida, A.; Cohen, B.; Asaka, T.; Kawai, A.; Organero, J. A.; Shibuya, K.; Douhal, A. Isomerization Dynamics of the 2-Phenylazo-1,3-Dimethylimidazolium Cation Photoexcited to the $S_2$ ($\pi,\pi^*$) State as Studied by Transient Absorption Spectroscopy in the Time Domain of $10^{-13}$ to $10^{3}$ Seconds. *Phys. Chem. Chem. Phys.* **2011**, *13*, 20318−20325.
(37) Wen, J.; Tian, Z.; Ma, J. Light- and Electric-Field-Induced Switching of Thiolated Azobenzene Self-Assembled Monolayer. *J. Phys. Chem. C* **2013**, *117*, 19934−19944.
(38) Miertuš, S.; Scrocco, E.; Tomasi, J. Electrostatic Interaction of a Solute with a Continuum. A Direct Utilizaion of Ab Initio Molecular Potentials for the Prevision of Solvent Effects. *Chem. Phys.* **1981**, *55*, 117−129.
(39) Tao, T.; Xu, F.; Chen, X.-C.; Liu, Q.-Q.; Huang, W.; You, X.-Z. Comparisons Between Azo Dyes and Schiff Bases Having the Same Benzothiazole/phenol Skeleton: Syntheses, Crystal Structures and Spectroscopic Properties. *Dyes Pigm.* **2012**, *92*, 916−922.
(40) Clifford, J. N.; Palomares, E.; Nazeeruddin, M. K.; Grätzel, M.; Nelson, J.; Li, X.; Long, N. J.; Durrant, J. R. Molecular Control of Recombination Dynamics in Dye-Sensitized Nanocrystalline $TiO_2$ Films: Free Energy Vs Distance Dependence. *J. Am. Chem. Soc.* **2004**, *126*, 5225−5233.
(41) Wu, Y.; Marszalek, M.; Zakeeruddin, S. M.; Zhang, Q.; Tian, H.; Grätzel, M.; Zhu, W. High-Conversion-Efficiency Organic Dye-Sensitized Solar Cells: Molecular Engineering on D−A−$\pi$-A Featured Organic Indoline Dyes. *Energy Environ. Sci.* **2012**, *5*, 8261.
(42) Kalyanasundaram, K. *Dye-Sensitized Solar Cells*; EPFL Press: Lausanne, Switzerland, 2010; p 19.
(43) Hara, K.; Sato, T.; Katoh, R.; Furube, A.; Yoshihara, T.; Murai, M.; Kurashige, M.; Ito, S.; Shinpo, A.; Suga, S.; et al. Novel Conjugated Organic Dyes for Efficient Dye-Sensitized Solar Cells. *Adv. Funct. Mater.* **2005**, *15*, 246−252.
(44) Lin, Y.-D.; Chow, T. J. Geometrical Effect of Stilbene on the Performance of Organic Dye-Sensitized Solar Cells. *J. Mater. Chem.* **2011**, *21*, 14907.